Structural Engineering and Mechanics, Vol. 38, No. 1 (2011) 81-97
DOI: http://dx.doi.org/10.12989/sem.2011.38.1.081

Wavelet-based damage detection method for a beam-type structure carrying moving mass

Hakan Gökdağ*

Department of Mechanical Engineering, Uludağ University, 16059 Görükle, Bursa, Turkey

(Received February 15, 2010, Accepted December 9, 2010)

Abstract. In this research, the wavelet transform is used to analyze time response of a cracked beam carrying moving mass for damage detection. In this respect, a new damage detection method based on the combined use of continuous and discrete wavelet transforms is proposed. It is shown that this method is more capable in making damage signature evident than the traditional two approaches based on direct investigation of the wavelet coefficients of structural response. By the proposed method, it is concluded that strain data outperforms displacement data at the same point in revealing damage signature. In addition, influence of moving mass-induced terms such as gravitational, Coriolis, centrifuge forces, and pure inertia force along the deflection direction to damage detection is investigated on a sample case. From this analysis it is concluded that centrifuge force has the most influence on making both displacement and strain data damage-sensitive. The Coriolis effect is the second to improve the damage-sensitivity of data. However, its impact is considerably less than the former. The rest, on the other hand, are observed to be insufficient alone.

Keywords: damage detection; wavelet transform; moving mass; cracked beam; strain.

1. Introduction

Structures under moving load constitute a significant field of research in engineering. They have important applications such as rails, railway bridges, runways, tunnels, pipelines, etc. Hence, many researches have been conducted to analyze dynamic behavior of them (Frýba 1999). The case of damaged beam subject to moving loads is, however, a recent issue. The earlier work on this topic appeared on the beginning of the century by Mahmoud (2001) to investigate the damage effect on structural response. In that paper, the author showed that crack shifts the minimum point of displacement profile to the right-hand on the time axis. Also, it was reported that a discontinuity appears in the slope of the deflected shape of the beam at the crack location. In a similar work, Mahmoud and Abu Zaid (2002) included the inertia effect of the moving load, and demonstrated that this is dominant at higher speeds on the time response. Later, Bilello and Bergman (2004) formulated the cracked beam under moving mass problem including all moving mass-related terms called as convective terms. The authors state that changes in time-response of the structure due to damage are more perceptible in comparison to the changes in the natural frequencies. Lin and

*Corresponding author, Ph.D., E-mail: hakangkd@uludag.edu.tr

Chang (2006), apart from the previous ones, derived the exact vibration modes of the cracked beam solving the relevant eigenvalue problem. Recently, Ariaei *et al.* (2009) modeled the cracked beam under moving load considering opening and closing of the crack during the load traverses beam. They included all of the convective terms, and solved the problem by both discrete element technique (DET) and the finite element method. The authors used the former method at the subsequent analyzes due to its less time-consuming property. From numerical applications, they concluded that breathing crack leads to less midspan deflection in comparison to the case of fully open crack. However, much more increase in the vibration amplitudes of the same point when moving load speed gets closer to the first critical speed is observed in the case of breathing crack.

Identifying damage location and, if possible, its extent are the issues as significant as understanding the impact of damage on the dynamics of structure. The wavelet transform (WT) is, in this regard, a proper technique for damage identification. The WT is a signal-processing tool widely used in data compression and singularity detection applications. Its performance on pinpointing singularity locations despite certain amount of noise interference has stimulated researchers to focus on wavelet-based damage detection methods (see, for example, Kim and Melhem (2004) for a literature survey). Some methods on this issue are based on analyzing the WT coefficients of the structural response in the form of spatial data such as vibration modes, static or dynamic displacement profiles. Certain derivatives of such data include local singularities at damage locations. The WT coefficients therefore form sharp peaks at these locations, and the magnitudes of these peaks are proportional to damage extent. There are two damage detection approaches by the WT coefficients (Gökdağ and Kopmaz 2009): In the first, only the WT coefficients of the response of the damaged structure are analyzed for damage evaluation. In the second, however, the WT coefficients of the response of healthy structure are also obtained, and, generally, subtracted from the former coefficients. This second method is more advantageous in the case of small-size damage (Zhong and Oyadiji 2007). However, if the number and extent of damage increase, this second approach loses its sensitivity. Moreover, healthy structural response as a reference data may not be available for many structures.

Zhu and Law (2006), using the above first approach, showed the possibility of identifying damage locations by the continuous WT. They demonstrated that the local time-dependent displacement response of a beam to moving load gains singularity at the time when moving load passes on the crack location. If the moving mass velocity is constant, then determining the singularity time means finding the damage location. Since the continuos WT coefficients of the displacement function are sensitive to local singularities, the peak points correspond to damage locations. From the parametric analyzes, they concluded that the WT coefficients are sensitive to the closeness of measuring point to damage location, the amount and the speed of moving force. Apart from that, in this research, a new wavelet-based damage detection method is proposed for beam carrying moving mass. This method does not necessitate the healthy structural response, and is based on using a suitable approximation function extracted from the initial data by the discrete WT (DWT) as reference. It is shown that the difference of the CWT coefficients of the initial data and the approximation function is more sensitive to damage than the previous two approaches. From the numerical simulations by the proposed method, it is concluded that strain data has more damage-sensitivity compared to displacement data. Moreover, apart from the work of Zhu and Law (2006), influence of moving mass-related terms such as gravitational force, Coriolis force, inertia force along the deflection direction, and the centrifuge force is investigated considering a specific example. It was observed that the centrifugal force has the most impact on making damage signature perceptible. The Coriolis force was the second despite not being as efficient as the former. The rest, on the contrary, were observed to be insufficient alone.

2. Theory

2.1 Dynamic response of a beam under moving load

Fig. 1 illustrates the system under consideration in this work, where a beam of length L with section sizes w and h is traversed by a moving mass of m_P with speed V_P. An open crack with height h_c is located at x_c. The crack is assumed to be fully open during the moving mass traverses beam. Moreover, moving mass and beam are assumed to be in contact throughout the motion. Furthermore, beam's surface roughness is neglected. In other words, the model adopted in references such as Mahmoud (2001), Zhu and Law (2006) is regarded. By the Euler-Bernoulli approach, the equation of motion of the beam can be given as (Rao 2000)

$$\rho A\frac{\partial^2 y}{\partial t^2}+C\frac{\partial y}{\partial t}+EI\frac{\partial^4 y}{\partial x^4}+m_P\delta(x-V_Pt)\left[V_P^2\frac{\partial^2 y}{\partial x^2}+2V_P\frac{\partial^2 y}{\partial x\partial t}+\frac{\partial^2 y}{\partial t^2}\right]=-m_Pg\delta(x-V_Pt) \tag{1}$$

where ρ, A, EI, and C denote, respectively, the density, section area, the bending stiffness, and viscous damping. δ is the Dirac delta function, and g means gravitational acceleration: $g = 9.81\ \mathrm{ms}^{-2}$. The first two terms in the bracket at the left side are centrifuge and Coriolis accelerations, respectively, whereas the third is the acceleration due to displacement along the vertical axis.

Mode superposition method can be used to solve the Eq. (1). To this end, free vibration modes of the undamped beam are obtained first. Setting C and m_P equal to zero, and introducing $y(x,t) = Y(x)\sin(\omega t)$ lead to the fourth-order homogeneous differential equation in $Y(x)$. The well-known solution is as follows

$$Y(x) = c_1\cos(\lambda x) + c_2\sin(\lambda x) + c_3\cosh(\lambda x) + c_4\sinh(\lambda x), \quad \lambda = (\rho A\omega^2/(EI))^{0.25} \tag{2}$$

where c_i $(i = 1, 2, 3, 4)$ denotes the undefined constants. The beam is assumed to be divided into two parts by the crack. Then, the compatibility equations at the crack location can be written as (Mahmoud 2001)

$$Y_1(x_c) = Y_2(x_c), \quad Y_1'(x_c)+\theta Y_1''(x_c) = Y_2'(x_c), \quad Y_1''(x_c) = Y_2''(x_c), \quad Y_1'''(x_c) = Y_2'''(x_c) \tag{3}$$

where subscripts 1 and 2 refer respectively to the beam portions at the left and right of the crack location. The first, third, and the fourth equations separated by comma in Eq. (3) imply the deflection, bending moment, and shear force continuity at the crack location while the second indicates slope discontinuity due to crack. The geometric factor θ is defined by

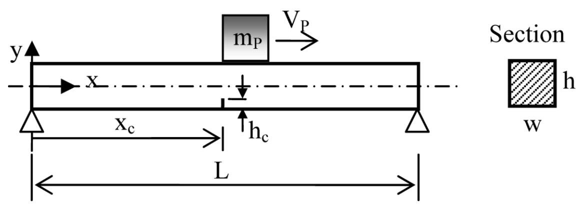

Fig. 1 Beam with a surface crack carrying a moving load

$$\theta = 2h\left(\frac{\bar{\delta}}{1-\bar{\delta}}\right)^2 (5.93 - 16.69\bar{\delta} + 37.14\bar{\delta}^2 - 35.84\bar{\delta}^3 + 13.12\bar{\delta}^4),\ \bar{\delta} = h_c/h \tag{4}$$

(Ariaei *et al.* 2009). Using Eq. (2), displacement, slope, curvature, and its derivative can be written in matrix notation as

$$\mathbf{V} = \mathbf{TC},\ \mathbf{V} = \begin{Bmatrix} Y(x) \\ Y'(x) \\ Y''(x) \\ Y'''(x) \end{Bmatrix},\ \mathbf{T} = \begin{bmatrix} \cos(\lambda x) & \sin(\lambda x) & \cosh(\lambda x) & \sinh(\lambda x) \\ -\lambda\sin(\lambda x) & \lambda\cos(\lambda x) & \lambda\sinh(\lambda x) & \lambda\cosh(\lambda x) \\ -\lambda^2\cos(\lambda x) & -\lambda^2\sin(\lambda x) & \lambda^2\cosh(\lambda x) & \lambda^2\sinh(\lambda x) \\ \lambda^3\sin(\lambda x) & -\lambda^3\cos(\lambda x) & \lambda^3\sinh(\lambda x) & \lambda^3\cosh(\lambda x) \end{bmatrix},\ \mathbf{C} = \begin{Bmatrix} c_1 \\ c_2 \\ c_3 \\ c_4 \end{Bmatrix} \tag{5}$$

Then, Eq. (3) becomes as follows

$$\mathbf{UV}_1 = \mathbf{V}_2 \Rightarrow \mathbf{UT}(x_c)\mathbf{C}_1 = \mathbf{T}(x_c)\mathbf{C}_2 \Rightarrow [\mathbf{UT}(x_c) - \mathbf{T}(x_c)]_{4\times 8}\begin{Bmatrix} \mathbf{C}_1 \\ \mathbf{C}_2 \end{Bmatrix}_{8\times 1} = \mathbf{0},\ \mathbf{U} = \begin{bmatrix} 1 & 0 & 0 & 0 \\ 0 & 1 & \theta & 0 \\ 0 & 0 & 1 & 0 \\ 0 & 0 & 0 & 1 \end{bmatrix} \tag{6}$$

where subscripts 1 and 2 again denotes, respectively, the first and the second beam parts separated by the crack. For each beam part, there are four c_i coefficients as seen in Eq. (2). In the case of single crack, one needs to define eight coefficients in total; the first four are the elements of the vector $\mathbf{C}_1$, and the rest belong to $\mathbf{C}_2$. Eq. (6) gives four equations. The remaining four are obtained by applying boundary conditions as $\mathbf{T}^L\mathbf{C}_1 = \mathbf{0}$ and $\mathbf{T}^R\mathbf{C}_2 = \mathbf{0}$, where $\mathbf{T}^L$ and $\mathbf{T}^R$ are 2×4 matrixes, L and R denotes, respectively, the points $x = 0$ and $x = L$. Finally, the following eigenvalue equation is obtained.

$$\begin{bmatrix} \mathbf{T}^L_{2\times 4} & \mathbf{0}_{2\times 4} \\ \multicolumn{2}{c}{\mathbf{T}^1} \\ \mathbf{0}_{2\times 4} & \mathbf{T}^R_{2\times 4} \end{bmatrix}_{8\times 8} \begin{Bmatrix} \mathbf{C}_1 \\ \mathbf{C}_2 \end{Bmatrix}_{8\times 1} = \mathbf{0},\qquad \mathbf{T}^1 = [\mathbf{UT}(x_c) - \mathbf{T}(x_c)]_{4\times 8} \tag{7}$$

If the number of crack is N_c, then there are $N_c + 1$ beam parts, hence Eq. (7) can be generalized as follows

$$\begin{bmatrix} \mathbf{T}^L_{2\times 4} & & & & & \mathbf{0} \\ & \mathbf{T}^1 & & & & \\ & & \mathbf{T}^2 & & & \\ & & & \cdots & & \\ & & & & \mathbf{T}^{N_c} & \\ \mathbf{0} & & & & & \mathbf{T}^R_{2\times 4} \end{bmatrix}_{4(N_c+1)\times 4(N_c+1)} \cdot \begin{Bmatrix} \mathbf{C}_1 \\ \mathbf{C}_2 \\ \cdot \\ \cdot \\ \cdot \\ \mathbf{C}_{N_c+1} \end{Bmatrix}_{4(N_c+1)\times 1} = \mathbf{0} \tag{8}$$

Solving the eigenvalue problem, the vibration modes (Y_i, $i = 1, 2, \ldots$) of the cracked beam is obtained (here the index "i" denotes the number of modes, and should not be confused with those in

Eqs. (3,6)). Then, the time response of a point on beam axis can be constituted as $y(x,t) = \Sigma_i Y_i(x) q_i(t)$. Substituting this into the Eq. (1), multiplying both sides by $Y_j(x)$, and integrating from 0 to L lead to the set of ordinary differential equations in modal coordinates $q_i(t)$, which can be represented by the state space form as

$$\mathbf{M}\ddot{\mathbf{q}} + \mathbf{C}\dot{\mathbf{q}} + \mathbf{K}\mathbf{q} = \mathbf{F} \Rightarrow \begin{Bmatrix} \dot{\mathbf{q}} \\ \ddot{\mathbf{q}} \end{Bmatrix} = \begin{bmatrix} \mathbf{0} & \mathbf{I} \\ -\mathbf{M}^{-1}\mathbf{K} & -\mathbf{M}^{-1}\mathbf{C} \end{bmatrix} \begin{Bmatrix} \mathbf{q} \\ \dot{\mathbf{q}} \end{Bmatrix} + \begin{Bmatrix} \mathbf{0} \\ \mathbf{F} \end{Bmatrix} \tag{9}$$

where the elements of the mass (**M**), stiffness (**K**), damping (**C**) matrixes as well as the generalized force vector (**F**) are defined as follows

$$M_{ij} = \int_0^L (\rho A Y_i Y_j + m_P \delta(x - V_P t) Y_i Y_j) dx, \quad C_{ij} = \int_0^L (C Y_i Y_j + 2 V_P m_P \delta(x - V_P t) Y_i' Y_j) dx$$

$$K_{ij} = \int_0^L (EIY_i'''' Y_j + V_P^2 m_P \delta(x - V_P t) Y_i'' Y_j) dx, \quad F_i = \int_0^L -m_P g \delta(x - V_P t) Y_j dx, \quad ' = d/dx \tag{10}$$

In this work, the ode45 function in MATLAB environment is employed to solve the Eq. (9) for the modal coordinates **q**. In addition to the time displacement of a point x, i.e., $y(x, t)$, one can obtain at the same point the strain ($\varepsilon_{xx}(x, t)$) of the beam's outer surface by the well-known stress-bending moment relation

$$\sigma_{xx} = E\varepsilon_{xx} = \frac{Mh}{2I} \Rightarrow E\varepsilon_{xx} = EI\frac{h}{2I}\frac{\partial^2 y}{\partial x^2} \Rightarrow \varepsilon_{xx}(x,t) = \frac{h}{2}\sum_i Y_i''(x) q_i(t) \tag{11}$$

where $M = EI\partial^2 y/\partial x^2$.

2.2 Basics of the wavelet transform

The CWT of a function $f(x) \in \mathbf{L}^2(|\mathbf{R})$ is defined by the integral

$$W(s,b) = s^{-1/2}\int_{-\infty}^{\infty} f(x)\,\psi_{s,b}(x) dx, \quad s, b \in |\mathbf{R}, \quad s > 0 \tag{12}$$

where $\psi_{s,b}(x)$ is derived from a mother wavelet $\psi(x)$ as $\psi_{s,b}(x) = \psi((x-b)/s)$ through the scale, s, and the shifting parameters, b. $\psi(x)$ is a compactly-supported, zero-mean function in $\mathbf{L}^2(|\mathbf{R})$, and satisfies some other mathematical requirements (Addison 2002). Moreover, $\psi(x)$ is said to have N vanishing moments if

$$\int_{-\infty}^{\infty} \psi(x) x^m dx = 0 \tag{13}$$

holds for $m = 0, 1, 2, \ldots, N-1$. As N increases, both the localization of the wavelet in x space and its regularity (i.e., differentialability) becomes better. This property is useful in damage detection applications. However, excessive number of vanishing moments (NVM) should be avoided, since the localization of wavelet decreases with increasing NVM. Otherwise, significant errors in pinpointing damage location occur. According to the relevant literature, N should be at least 2. However, $N = 4$ and $N = 6$ are preferred frequently due to the practical concerns such as noise interference (Hong *et al.* 2002, Loutridis *et al.* 2005, Gökdağ 2008).

If the scale and shifting parameters in Eq. (12) are sampled as $s = 2^j$, $b = n2^j$, which is called as dyadic sampling, and if an orthogonal wavelet is used, then the DWT coefficients $W_{j,n}$ are obtained. In this case, it is possible to decompose $f(x)$ to an approximation function at the J^{th} decomposition level, $A_J(x)$, and the sum of detail functions $D_j(x)$ up to that level as (Addison 2002)

$$f(x) = A_J(x) + \sum_{j=-\infty}^{J} D_j(x), \quad D_j(x) = \sum_{n=-\infty}^{\infty} W_{j,n}\psi_{j,n}(x) \tag{14}$$

Here, A_J represents the smooth part of $f(x)$ whereas the sum of the details includes the higher frequency variations. A_J becomes smoother with increasing J.

Although the DWT coefficients can also be employed for damage detection, the CWT is preferred mostly due to its redundancy feature that improves the damage sensitivity of the WT coefficients (Douka *et al.* 2003). In this work, the CWT-based indexes are used for damage detection.

2.3 The proposed damage detection method

Suppose that the time displacement of a point a $(0 \le a \le L)$ or the time-dependent strain at the same point be $f(t)$; i.e., $f(t) = y(a, t)$ or $f(t) = \varepsilon_{xx}(a, t)$. Then, the WT coefficients of this function are to be computed. In this case, the parameter x in Eq. (12) is replaced with t. Before extracting a suitable approximation function $(A_J(t))$ from $f(t)$, $f(t)$ needs to be extended at the ends to reduce boundary distortion. This is of significant importance for the proper application of the proposed method. There are several approaches for this operation such as symmetric, antisymmetric, periodic extensions, and extension by cubic spline extrapolation (Messina 2008, Loutridis *et al.* 2005, Rucka and Wild 2006). Moreover, other easily applicable methods such as zeropad, smooth padding can be cited (Misiti *et al.* 2007), as well. However, none of these is suitable for every boundary type. Moreover, the extrapolation-based ones are sensitive to noise interference. Messina (2008), to avoid such restrictions, developed an optimization-based procedure that can significantly reduce distortions even in the general case of unknown boundary types and noisy data. According to his method, data is first extended at the ends by global polynomial fit (i.e., using all data points), which is called as first approximation. Later, this approximation is further refined by adjusting polynomial coefficients through an optimization procedure. The objective function of this procedure is the norm of the wavelet coefficients inside the interval influenced by distortions around the initial data ends. Despite its efficiency, this method consumes considerable time in comparison to the previous ones. Moreover, it needs a bit complex programming. In this research, an easily applicable and efficient way that is just based on polynomial extension is proposed. Two issues that considerably affect the success of this method are the degree of the extension polynomial (D) and the number of points considered in the curve fitting procedure (N_{cf}). D depends on the NVM of the selected wavelet for extension. If data is extended at an end by a wavelet with N NVM, then D should be equal to $N-1$ according to the Eq. (13), since the wavelet can only be orthogonal to the polynomials up to the degree $N-1$. When D is more or less, some derivatives at the end may be discontinuous, which in turn may yield additional distortions. On the other hand, the suitable N_{cf} is determined after D is decided. One can experience that distortions vary in a large range depending on N_{cf}. It is difficult to state a certain rule for the suitable N_{cf}. However, to the authors experience with many data, the suitable N_{cf} is generally obtained in the interval $D + 1 \le N_{cf} \le 0.3N_m$, where N_m denotes the initial length of the data to be extended (note that at least $D + 1$ data points are required if a polynomial of degree D is fitted). Regarding each N_{cf} in this interval, the following norm is computed to find out quantitative measure of distortions, and the N_{cf} that corresponds to the minimum distortion is selected.

$$F_{l,r} = \left(\sum_{i = N_{l,r} - R(0.25sN_{sp})}^{N_{l,r} + R(0.25sN_{sp})} W(s,i)^2 \right)^{1/2} \quad l\text{: left end, } r\text{: right end} \tag{15}$$

where $N_l = N_e$, and $N_r = N_e + N_m$, if data of length N_m is extended by adding N_e terms at each end. In this paper, the symlet family is regarded. Its support length is $N_{sp} = 2N-1$, where N is NVM (Misiti *et al.* 2007). For this wavelet, the length of the interval including the significant nonzero terms is nearly half of its full support length. Therefore, the intervals $[N_e - R(s0.25N_{sp}), N_e + R(s0.25N_{sp})]$ and $[N_e + N_m - R(s0.25N_{sp}), N_e + N_m + R(s0.25N_{sp})]$, where $R(\cdot)$ means rounding to the nearest integer, should be regarded for the left and right ends, respectively, if extension is performed at scale s.

When moving mass passes over the damage point (i.e., when $V_P t = x_c$ is realized), a local discontinuity arises in $f(t)$ (Zhu and Law 2006). The purpose is to detect this by the CWT coefficients of the extended $f(t)$. However, $f(t)$ has less sensitivity to such local singularity in comparison to vibration modes. Hence, only the examination of CWT coefficients of $f(t)$ may not be helpful in identifying damage location, particularly in the case of small-size damage. Therefore, a new and more sensitive damage index whose application will be set forth shortly is proposed here. The assumption that this new method is based on is that the CWT coefficients of the difference $f(t) - A_J(t)$ are sensitive to local singularity, where $A_J(t)$ is a suitable approximation function extracted from $f(t)$ by the DWT. Here, the suitable $A_J(t)$ is assumed to be both extremely compatible with $f(t)$ and considerably free of local singularities. The compatibility of $f(t)$ and $A_J(t)$ can be measured quantitatively by the well-known modal assurance criterion (MAC) (Ewins 2000). Since $f(t)$ and $A_J(t)$ are represented by vectors of discrete numbers in the computer environment, the MAC between them can be computed by

$$0 \le \mathrm{MAC}(A_J, f) = \left(\sum_k A_J(k) f(k)\right)^2 \Big/ \left(\sum_k A_J^2(k) \sum_k f^2(k)\right) \le 1 \qquad k = 1, 2, \ldots, K \tag{16}$$

where K is the length of each vector. To achieve higher MAC, $A_J(t)$ should be extracted from $f(t)$ using a wavelet with large NVM (Gökdağ and Kopmaz 2010). Because the frequency spectrum of the scale function of the mother wavelet becomes narrower about zero frequency axis (Debnath 2002), which means the scale function of the wavelet becomes more sensitive to lower-frequency parts. $A_J(t)$ contains, as stated previously, the lower-frequency parts of $f(t)$. Hence, processing $f(t)$ with a wavelet with larger NVM enables to obtain $A_J(t)$ that is more compatible with $f(t)$. Then, the question of how high the NVM should be arises. The Fig. 3.15 in Addison (2002) is helpful to determine the suitable interval for NVM. It can be verified by this figure at the reference work that the shrinkage of the scale function of the Daubechies (Db) wavelet becomes negligible when its NVM satisfies the condition $10 \le \mathrm{NVM} \le 20$. The properties of the symlet family are similar to those of Db wavelets (Misiti *et al.* 2007), as well. Moreover, its symmetry, which is desired to achieve better visual representation, is better than Db wavelets. Hence, it is proposed here that a symlet with NVM between the interval [10,20] can be employed in the DWT to extract suitable $A_J(t)$.

After deciding on the proper wavelet to use in the DWT, the appropriate DWT decomposition level should be determined. As J increases, $A_J(t)$ becomes more free of singularity-like variations, hence the MAC decreases slightly. However, after a certain J, which mostly depends on the data length, the MAC drops sharply. Because, not only the high-frequency signal components that include both damage-induced singularities and high-frequency noise parts are removed from $f(t)$, but also some basic lower-frequency components having significant contribution to the general form of $f(t)$ are begun to be removed. This situation implies that J should not be increased further.

In the light of the previous explanations, the steps of the method can be ordered as follows:

1) Extend $f(t)$ in the way proposed. The wavelet to be used for extension should be the same with the one that will be used to compute the CWT-based damage index. Avoid from excessively small scales for the sake of stability of numerical operations (Messina 2008).
2) Select a sym$N$ wavelet with $N \geq 10$, where N denotes NVM, and compute MAC for the first several J levels. Determine the decomposition level where the first notable drop in the MAC is observed. Then, the approximation function before this level can be taken as the suitable one.
3) Compute the following damage index with the extended $f(t)$ and the $A_J(t)$ extracted from $f(t)$ at the second step

$$I_I = W_f(s, b) - W_A(s, b) \tag{17}$$

where W_f and W_A refers, respectively, to the CWT coefficients of $f(t)$ and $A_J(t)$.

For the purpose of comparison, the following indexes will also be computed

$$I_{II} = W_f(s, b) - W_f^u(s, b), \quad I_{III} = W_f(s, b) \tag{18}$$

where upper u indicates the CWT coefficients of the time-dependent response of the healthy beam. Note that I_I employs a reference data as well as I_{II}. However, I_I extracts this from the damaged structural response by the DWT.

3. Numerical applications

3.1 Model verification

First, the reliability of the model used to obtain time response data will be tested. To this end, the following data considered by Ariaei *et al.* (2009) is employed to obtain the time displacement of beam midspan: $L = 50$ m, $\rho = 7860$ kgm^{-3}, $w = 0.5$ m, $h = 1$ m, $m_P = 39300$ kg (equal to 20 percent of the beam mass), $g = 9.81$ ms^{-2}, $x_c = 0.5L$ and $\bar{\delta} = 0.5$. The first six vibration modes are employed, and the sampling frequency is taken as 1000 Hz, which is sufficiently more than the 2.5 times of the 6th natural frequency of the beam (~34 Hz). Besides 2 percent modal damping is assumed as in Zhu and Law (2006).

Fig. 2 shows the time displacement of the midspan for different moving mass speeds. Comparing this with the Fig. 5 in Ariaei *et al.* (2009), one can realize the general agreement between them. However, at higher speeds there occur some discrepancies between the curves. For example, the minimum point at Fig. 2 for $V_P = 80$ ms^{-1} is -2.15 whereas it is nearly -2 in the Fig. 5 of the reference paper. Similarly, at $V_P = 160$ ms^{-1} the minimum points are -0.81(here) and approximately -0.6(reference). That is, discrepancy becomes significant with increasing speed. This may be due to the approaches to obtain vibration modes. In the reference work, the DET is used. The accuracy of this depends on the number of discrete elements. However, the exact vibration modes of the beam are employed in the present work.

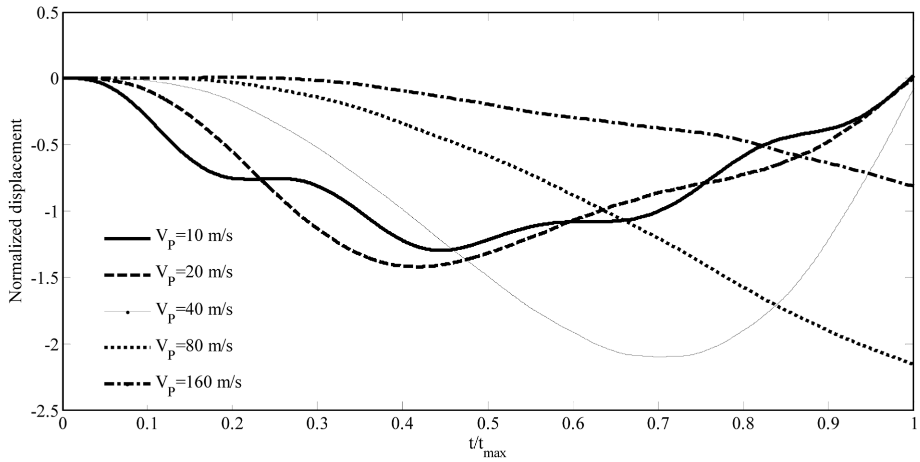

Fig. 2 Time-dependent displacements of beam midspan for various moving mass speeds. Normalization is performed by dividing each data to $m_P g L^3/48EI$, i.e., the static displacement of the midspan under the load $m_P g$

Table 1 Comparison of distortions by several methods for various scales

Scale (s)		Pol	Asym	Sym	Per	CSE
2	F_l	1.67×10^{-5}	3.09×10^{-5}	2.06×10^{-5}	2.37×10^{-3}	3.45×10^{-5}
	e_l	---	85	23	>100	>100
	F_r	6.91×10^{-6}	1.59×10^{-5}	1.25×10^{-3}	2.37×10^{-3}	7.2210^{-6}
	e_r	---	>100	>100	>100	4
6	F_l	8.76×10^{-5}	1.58×10^{-4}	1.44×10^{-4}	9.63×10^{-3}	7.73×10^{-4}
	e_l	---	80	64	>100	>100
	F_r	2.92×10^{-5}	7.21×10^{-5}	1.07×10^{-2}	9.63×10^{-3}	3.09×10^{-3}
	e_r	---	>100	>100	>100	>100
10	F_l	5.74×10^{-5}	1.25×10^{-4}	9.88×10^{-5}	1.99×10^{-2}	2.35×10^{-3}
	e_l	---	>100	72	>100	>100
	F_r	1.42×10^{-4}	4.95×10^{-4}	2.99×10^{-2}	1.99×10^{-2}	5.13×10^{-3}
	e_r	---	>100	>100	>100	>100
20	F_l	6.59×10^{-4}	1.45×10^{-3}	1.29×10^{-3}	6.49×10^{-2}	9.69×10^{-2}
	e_l	---	>100	96	>100	>100
	F_r	5.09×10^{-3}	1.44×10^{-2}	1.21×10^{-1}	6.49×10^{-2}	1.83×10^{-1}
	e_r	---	>100	>100	>100	>100

"*l*": left, "*r*": right, Pol: Polynomial (proposed), Asym: Antisymmetric, Sym: Symmetric, Per: Periodic, CSE: Cubic Spline Extrapolation, $e = 100(F^* - F_{Pol})/F_{Pol}$, F^*: one of the four methods other than Pol. The wavelet used for extension is sym6, so that fifth-degree polynomials are employed in the Pol method.

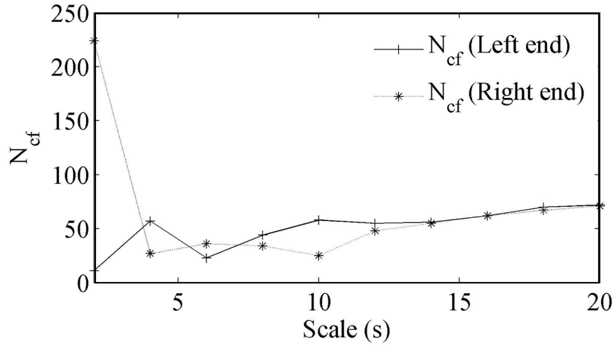

Fig. 3 Variation of the suitable N_{cf} wrt scale

3.2 Performance of the proposed boundary extension method

Let's consider the time displacement of the midspan of the same beam for the speed $V_P = 20$ m/s (other values are the same if otherwise not stated). The data is assumed to be contaminated by white noise such that the signal to noise ratio (SNR) is 100 dB. Table 1 compares the distortions at various scales by several methods including the proposed one. As can be easily seen, the least distortion at every case is achieved by the proposed polynomial method (Pol). The relative errors, taking the Pol as reference, are given for comparison. Errors more than 100 percent are shown by >100. It is observed that the present method yields considerably smaller distortions, hence can be acknowledged as the most efficient. On the other hand, Fig. 3 illustrates the variation of the suitable N_{cf} values for the left and right end of the time data. The time data is sampled at 1000 Hz, and the total time for the moving mass to move along the beam is $L/V_P = 50/20 = 2.5$ s. Therefore, the length of the time data is $N_m = 2500$. Fig. 2 verifies that the suitable N_{cf} is always smaller than $0.3N_m = 750$. Moreover, as the scale increases, the suitable N_{cf} values for each data end becomes closer, which can be ascribed to the stability of numerical operations at higher scales.

3.3 Performance of the proposed damage index (I_I)

The same beam is considered again. To indicate the application of the proposed damage detection method, this time two damages are assumed to exist at the points $x_{c1} = 0.3L$, $x_{c2} = 0.7L$ with $\bar{\delta}_1 = \bar{\delta}_2 = 0.2$. The moving mass speed is $V_P = 20$ ms^{-1}, and the other parameters remain the same. The time-dependent displacement and strain of the midspan are illustrated in Fig. 4. It is seen that damage slightly changes both data.

Again white noise is added to contaminate both data such that SNR = 100 dB. The extension is performed at the 10th scale, i.e., $s = 10$, which is sufficiently large for damage effect to become evident, by using sym6 wavelet whose NVM equals to 5. To extract a suitable approximation function by the DWT, the sym18 wavelet is employed. Table 2 shows variation of the MAC wrt the DWT decomposition level J. From the table, the MAC is seen to decrease slightly with increasing J. However, after a certain value, which is $J = 4$ for the displacement, and $J = 3$ for the strain, a sharp drop is observed. Then, it can be concluded that the suitable levels for displacement and strain data are $J = 4$ and $J = 3$, respectively. Indeed, this conclusion is more obvious in Fig. 5, where I_I indexes around these levels are illustrated by colormap representation. Since the displacement data

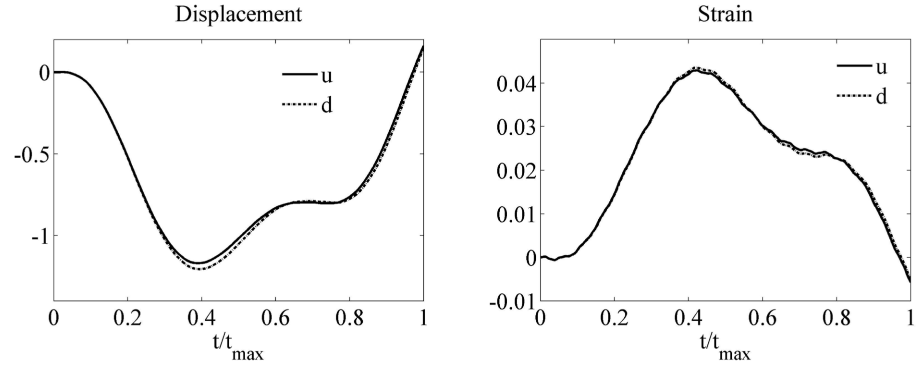

Fig. 4 Normalized time-dependent displacements and strains of the beam midspan in healthy and damaged cases. Each strain data is divided by the static strain $e_{static} = m_P gLh/8EI$ for normalization. *u*: undamaged, *d*: damaged

Table 2 MAC versus DWT decomposition level (*J*). sym18 is used to obtain approximation functions

	MAC	
J	Displacement	Strain
1	0.99999999998800	0.99999999998548
2	0.99999999998208	0.99999999997798
3	0.99999999997927	**0.99999999996341**
4	**0.99999999994775**	0.99999998755777
5	0.99999999754260	0.99999869533762
6	0.99999974883043	0.99993498143988

is not as sensitive to damage as the strain data, let's explain the scene in Fig. 5 regarding the strain data. In the right column of Fig. 5, where the approximation function at the second level is used to obtain I_I, it is observed that the index is not sufficient in revealing damage-induced singularities. The reason is that $A_2(t)$ is not sufficiently free of such singularities. As I_I is based on the difference $f(t) - A_2(t)$, these singularites cancel out each other, so that I_I can not reveal damage signature. On the other hand, when $A_4(t)$ is regarded, the formal resemblance of $f(t)$ and $A_4(t)$ diminishes, so that the sensitivity of I_I to damage drops significantly. In the case of $A_3(t)$, however, both damages are obviously seen.

In Fig. 6 colormap representations of the indexes I_{II} and I_{III} are displayed. Damage signature can barely be perceived in these graphs. Comparison of the indexes at the 10th scale (see Fig. 7) highlights the efficiency of the index I_I. Hence, I_I is regarded for the subsequent analysis.

3.4 Effects of moving mass force terms on damage detection

This time damage locations are as follows: $x_{c1} = 0.3L$, $x_{c2} = 0.7L$, $x_{c3} = 0.85L$. According to the previous analyzes the displacement data is less sensitive to damage. Therefore, moderate crack depth ($\bar{\delta}_1 = \bar{\delta}_2 = \bar{\delta}_3 = 0.4$) is considered this time for better evaluation of the impact of moving mass-related force terms on the performance of damage detection. To this end, the cases in Table 3 are regarded, and the corresponding time data are displayed in Fig. 8. According to the figure, the

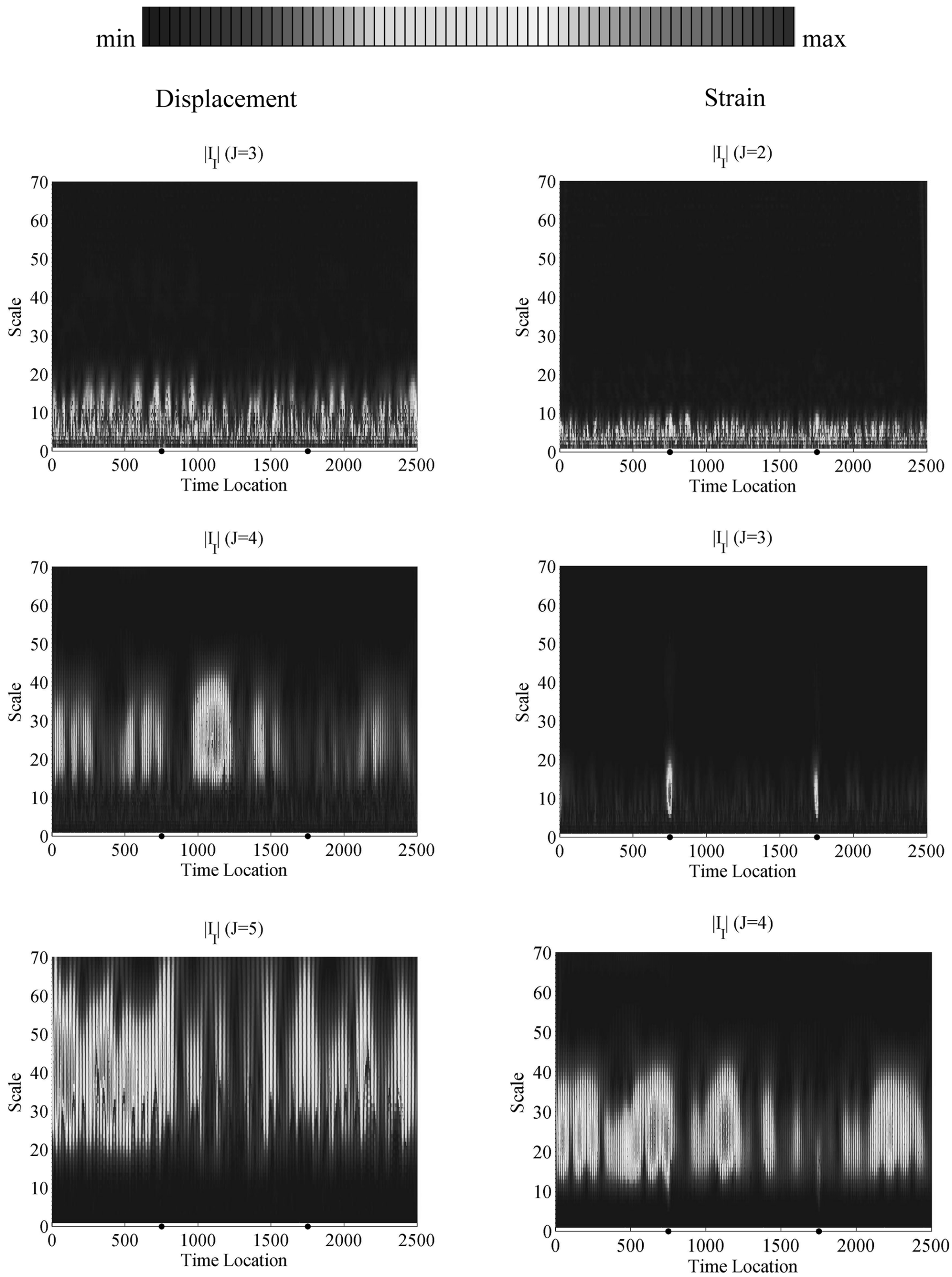

Fig. 5 I_I index for displacement (left column) and strain (right column) data at various decomposition levels (J). Black dots on the horizontal axis denote damage locations at $0.3L$ and $0.7L$

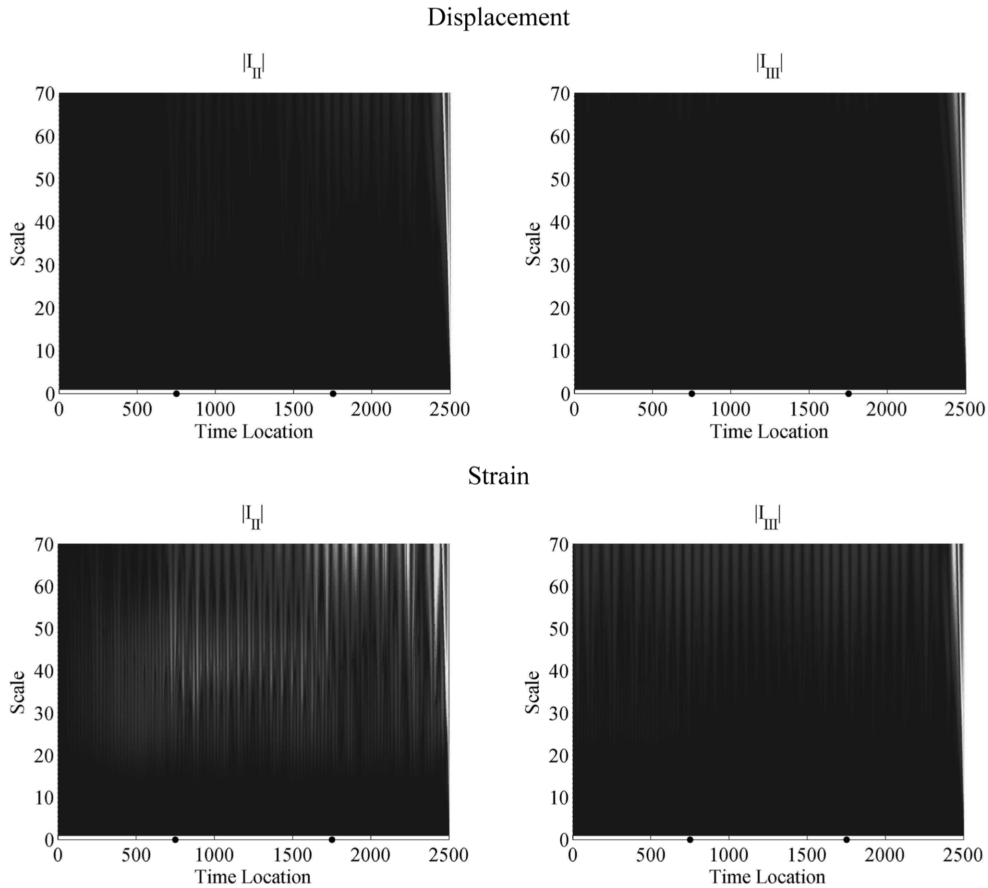

Fig. 6 Colormap representation of I_{II} and I_{III} indexes for displacement and strain data

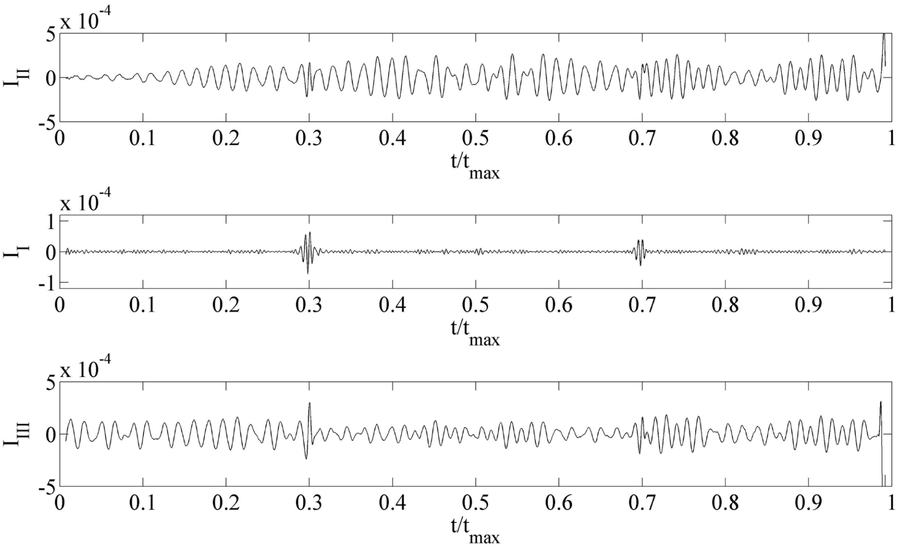

Fig. 7 Comparison of the damage indexes at the 10th scale

Table 3 Considered cases for the evaluation of influence of moving mass-related terms on damage detection performance. +: included, –: not included, subscript "*x*" and "*t*" denote partial derivatives wrt those variables

Case	Moving Force $-m_P g\delta(x - V_P t)$	Inertia Force $m_P\delta(x - V_P t) \cdot y_{tt}$	Coriolis Force $m_P\delta(x - V_P t) \cdot 2V_P y_{xt}$	Centrifuge Force $m_P\delta(x - V_P t) \cdot V_P^2 y_{xx}$
1	+	–	–	–
2	+	+	–	–
3	+	–	+	–
4	+	–	–	+
5	+	+	+	+
6	+	–	+	+

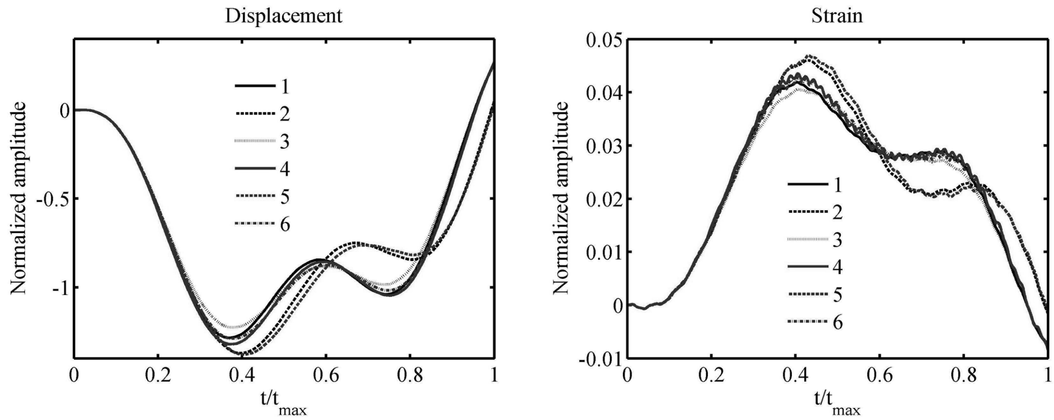

Fig. 8 Midspan displacement and strain curves for each case in Table 3, $V_P = 20$ ms^{-1}

curves corresponding to the cases 2 and 5 exhibit a close trend. Similarly, the remaining curves show resemblance among themselves. On the other hand, the plot of I_I for each case is given in Fig. 9. Damage effects were experienced to be sufficiently evident at the 10th and 20th scales for strain and displacement data, respectively. Therefore, only these scales are regarded. According to the plots for the strain data, damage signatures are extremely obvious in the cases 4,5, and 6. On the other hand, the best results are obtained at the 4th and 6th cases for the displacement data. In the latter plots, the index exhibits a large-magnitude peak at the second damage location (0.7L) while it suddenly increases and decreases at the first (0.3L) and third (0.85L) damage locations, respectively. That is, the first and third damage locations are indirectly detected whereas the second damage location is directly determined. The following conclusions can be drawn from the complete evaluation of Fig. 9:

1) Both centrifuge and Coriolis forces improve damage sensitivity of the index I_I. However, centrifuge force has relatively more contribution.
2) Case 5 corresponds to the real situation where all of the moving-mass related terms exist. Case 6 excludes the vertical inertia effect. Although insignificant change is observed for strain data, I_I exhibits better result in Case 6 than Case 5. This means the vertical inertia force due to the

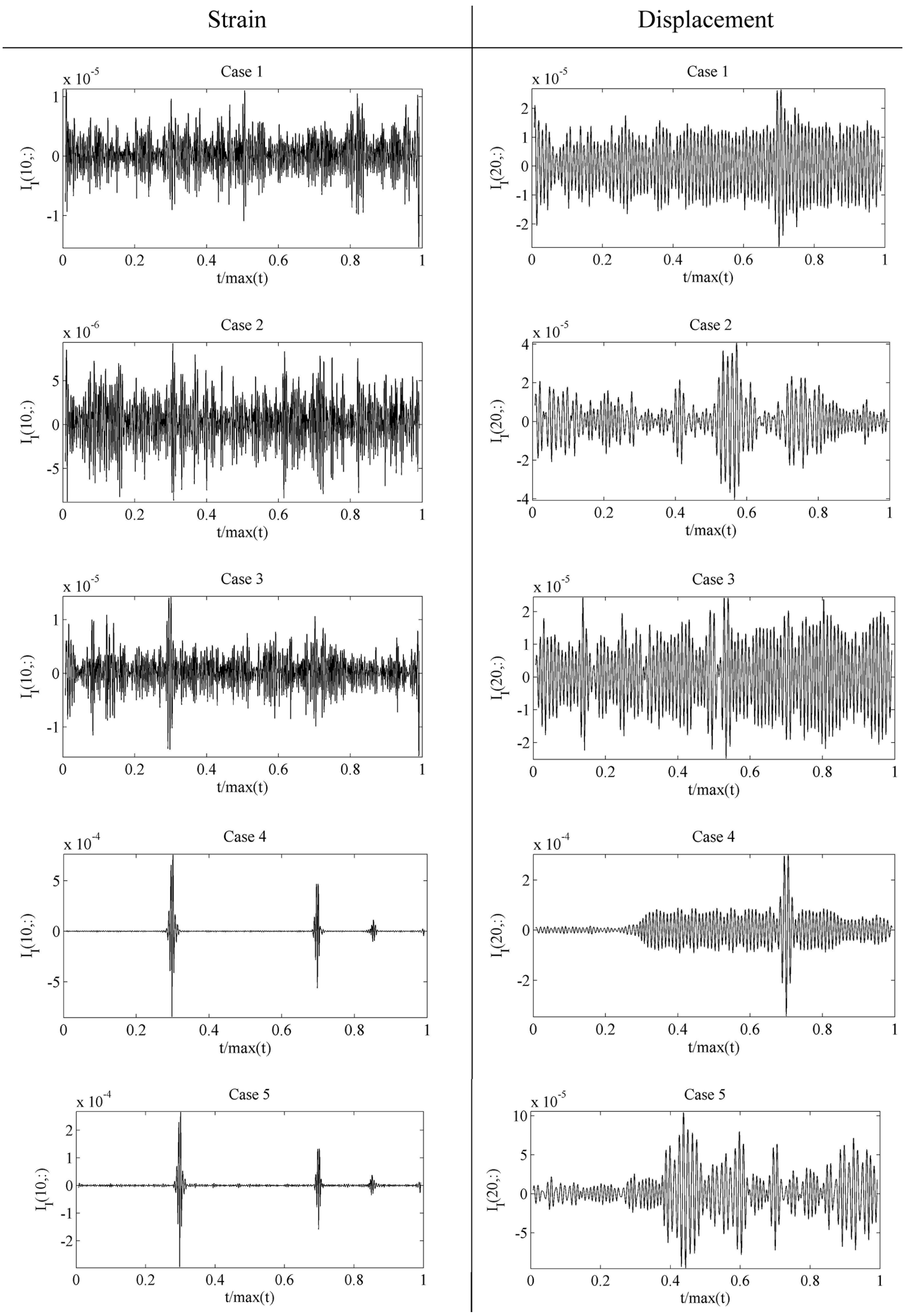

Fig. 9 Damage detection results for the cases in Table 3

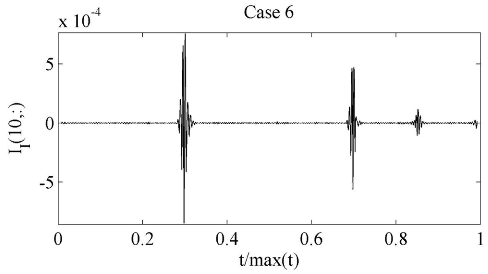

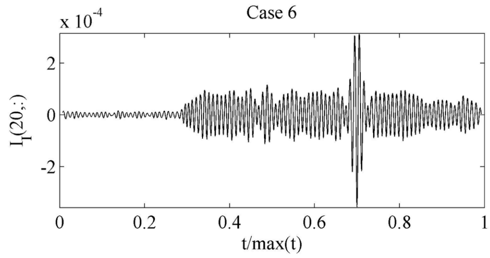

Fig. 9 Continued

moving mass adversely affects the damage sensitivity of I_I. However, this conclusion may not be valid for other m_P, V_P values, and crack locations and extents.

3) The strain data is considerably more sensitive to damage than displacement. Hence, in practical applications strain data can be used to get reliable results.

4. Conclusions

In this research, time data measured from a point on a beam under moving load is analyzed by the WT to identify damage locations. In this respect, a new method whose performance is superior to the two methods that are based on direct investigation of the CWT coefficients of data is introduced. This new method is based on the combined use of the CWT and the DWT. According to the method, the data measured from damaged structure is first extended to reduce boundary distortion. In this regard, a new technique based on just polynomial extension is proposed. It was shown that this method is relatively more efficient than the other frequently-used approaches. Later, a suitable approximation function is extracted from the extended data by the DWT, and a sensitive damage index is defined by the difference of the CWT coefficients of the original data and its approximation function. From the numerical applications, it was concluded that strain data is more sensitive to damage than displacement. Moreover, the centrifuge and Coriolis forces among the moving mass-related force terms are experienced to improve the damage detection performance of the damage index. Numerical and experimental evaluations of the performance of the proposed damage index for various m_P and V_P values, damage locations, data measurement points are worthy of further investigation. Moreover, damage models including crack's opening and closing, load-beam interaction etc should be regarded in modeling to produce more realistic time data. Hence, the future works are planned to cover these topics.

References

Addison, P.S. (2002), *The Illustrated Wavelet Transform Handbook: Introductory Theory and Applications in Science, Engineering, Medicine and Finance*, IOP Publishing Ltd., London.

Ariaei, A., Ziaei-Rad, S. and Ghayour, M. (2009), "Vibration analysis of beams with open and breathing cracks subjected to moving masses", *J. Sound Vib.*, **326**, 709-724.

Bilello, C. and Bergman, L.A. (2004), "Vibration of damaged beam under a moving mass: theory and experimental validation", *J. Sound Vib.*, **274**, 567-582.

Debnath, L. (2002), *Wavelet Transforms and Their Applications*, Birkhäuser, Boston.

Douka, E., Loutridis, S. and Trochidis, A. (2003), "Crack identification in beams using wavelet analysis", *Int. J. Solids Struct.,* **40**, 3557-3569.

Ewins, D.J. (2000), *Modal Testing: Theory, Practice and Applications*, Research Studies Press Ltd., Baldock.

Frýba, L. (1999), *Vibration of Solids and Structures Under Moving Loads*, Thomas Telford Ltd., Prague.

Gökdağ, H. (2008), "Application of continuous wavelet transform to detect damage in thin-walled beams coupled in bending and torsion", *Struct. Eng. Mech.,* **29**(3), 351-354.

Gökdağ, H. and Kopmaz, O. (2009), "A new damage detection approach for beam-type structures based on the combination of continuous and discrete wavelet transforms", *J. Sound Vib.*, **324**, 1158-1180.

Gökdağ, H. and Kopmaz, O. (2010), "A new structural damage detection index based on analyzing vibration modes by the wavelet transform", *Struct. Eng. Mech.,* **35**(2), 257-260.

Hong, J.C., Kim, Y.Y., Lee, H.C. and Lee, Y.W. (2002), "Damage detection using the Lipschitz exponent estimated by the wavelet transform: applications to vibration modes of a beam", *Int. J. Solids Struct.,* **39**, 1803-1816.

Kim, H. and Melhem, H. (2004), "Damage detection of structures by wavelet analysis", *Eng. Struct.*, **26**, 347-362.

Lin, H.P. and Chang, S.C. (2006), "Forced responses of cracked cantilever beams subjected to a concentrated moving load", *Int. J. Mech. Sci.*, **48**, 1456-1463.

Loutridis, S., Douka, E., Hadjileontiadis, L.J. and Trochidis, A. (2005), "A two-dimensional wavelet transform for detection of cracks in plates", *Eng. Struct.*, **27**, 1327-1338.

Mahmoud, M.A. (2001), "Effect of cracks on the dynamic response of a simple beam subject to a moving load", *Proc. Ins. Mech. Eng.,* **215**, 207-215.

Mahmoud, M.A. and Abou Zaid, M.A. (2002), "Dynamic response of a beam with a crack subject to a moving load", *J. Sound Vib.*, **256**(4), 591-603.

Messina, A. (2008), "Refinements of damage detection methods based on wavelet analysis of dynamical shapes", *Int. J. Solids Struct.,* **45**, 4068-4097.

Misiti, M., Misiti, Y., Oppenheim, G. and Poggi, J. (2007), *Wavelet Toolbox 4 (Ver. 4.1 Rel.2007b) Use's Guide*, Natick, The MathWorks, MA, USA.

Rao, G.V. (2000), "Linear dynamics of an elastic beam under moving loads", *J. Vib. Acoust.-ASME*, **122**, 281-289.

Rucka, M. and Wilde, K. (2006), "Application of continuous wavelet transform in vibration based damage detection method for beams and plates", *J. Sound Vib.*, **297**, 536-550.

Zhong, S. and Oyadiji, O. (2007), "Crack detection in simply supported beams without baseline modal parameters by stationary wavelet transform", *Mech. Syst. Signal Pr.,* **21**, 1853-1884.

Zhu, X.Q. and Law, S.S. (2006), "Wavelet-based crack identification of bridge beam from operational deflection time history", *Int. J. Solids Struct.,* **43**, 2299-2317.